Submitted to Geophysics Research Letters on October 7, 2010

Terrestrial Myriametric Radio Burst Observed by *IMAGE* and *Geotail* Satellites

Shing F. Fung[1], Kozo Hashimoto[2], Scott A. Boardsen[3], Leonard N. Garcia[4], James L. Green[5], Hiroshi Matsumoto[6], and Bodo W. Reinisch[7]

[1]Geospace Physics Laboratory, NASA Goddard Space Flight Center, Greenbelt MD

[2]Paleological Association of Japan, Inc., Kyoto, Japan

[3]UMBC, NASA Goddard Space Flight Center, Greenbelt MD

[4]Wyle, NASA Goddard Space Flight Center, Greenbelt MD

[5]Planetary Science Division, NASA Headquarters, Washington D.C.

[6]Headquarters, Kyoto University, Kyoto, Japan

[7]Lowell Digisonde International, Lowell MA

Abstract

We report *IMAGE* and *Geotail* simultaneous observations of a terrestrial myriametric radio burst (*TMRB*) detected on August 19, 2001. The *TMRB* was confined in time (0830-1006 UT) and frequency (12-50 kHz), suggesting a fan beam-like emission pattern from a single discrete source. Analysis and comparisons with existing *TMR* radiations strongly suggest that the *TMRB* is a distinct emission perhaps resulting from dayside magnetic reconnection instigated by northward interplanetary field condition.

Introduction

Myriametric radio emissions (with wavelengths of 10-100 km) from Earth's magnetosphere have been known to take on different forms. Most notable forms include the classical non-thermal continuum (*NTC*) with both escaping and trapped components, continuum enhancement (*CE*), and auroral myriametric radiation (*AMR*). Continuum radiation emanating from plasmaspheric notches at the magnetic equator can sometimes extend to higher frequencies (up to ~ 800 kHz) to form the so-called kilometric continuum (*KC*) radiation. *CE* has also been known to appear as low-frequency bursts associated with substorm particle injections. This paper presents the simultaneous *IMAGE* and *Geotail* observations of a burst of terrestrial myriametric radiation (*TMRB*) at 8:30-10:06 UT on August 19, 2001. The widely separated satellite observations at 12-50 kHz suggest that the *TMRB* was a temporal feature. We will compare the *TMRB* observations to the characteristics of other known *TMR* components to determine if the *TMRB* may be consistent with any of the known *TMR*.

Observations of Terrestrial Myriametric Radio Burst (TMRB)

a) Spacecraft locations

On August 19, 2001, 0830-1006 UT, the *IMAGE* satellite was near apogee (R ~ 8 Re) over the northern polar region in the afternoon sector while *Geotail* was at perigee (R ~ 9 Re) located just north of the magnetic equator in the post-midnight/pre-dawn sector. Using the *NASA SSCWeb* tool (*http://sscweb.gsfc.nasa.gov*), we show in Figure 1 the *IMAGE* and *Geotail* positions in *GSM* X-Y plane during the times of *TMRB* observations.

The *IMAGE* and *Geotail GSM* coordinates indicate that the two satellites were situated on opposite sides of Earth, nearly along an afternoon-early morning meridian plane. *IMAGE*, however, was at much-higher geomagnetic latitudes (71.81°-80.46°) than *Geotail* (7.98°-12.35°). The difference in geomagnetic longitudes shown in Figure 1 means that the two satellites are situated on essentially diametrically opposite field lines. Over this interval, the geomagnetic longitude of *IMAGE* changed by ~11°, while that of *Geotail* was ~ -5.3°.

b) *IMAGE* and *Geotail* observations

Figure 2 shows the 6-hour dynamic spectrograms for August 19, 2001, recorded by the *IMAGE Radio Plasma Imager* (*RPI*, lower panel) [*Reinisch et al.*, 2000] and *Geotail Plasma Wave Instrument* (*PWI*, upper panel) [*Matsumoto et al.*, 1994]. The emission feature at 12-50 kHz observed simultaneously by both satellites at 0830-1006 UT (demarcated by the two white lines) is identified here as the terrestrial myriametric radio burst (*TMRB*). Given the widely separated spacecraft locations, the start and stop of the *TMRB* being seen simultaneously by both satellites strongly suggest that the *TMRB* was turning on and off, just like a light bulb.

In view of the differences in spacecraft locations, it is of interest to contrast the wave signatures between the two spectrograms in Figure 2. Firstly, the *TMRB* observed by both satellites appears as an isolated magnetospheric emission with an enhancement near the center of the burst. The simultaneous observations of the *TMRB* when *IMAGE* and *Geotail* were fortuitously located at different latitudes on diametrically opposite sides of the Earth suggest that the *TMRB* must at a minimum have a fan-beam radiation pattern that covers the latitude and longitude ranges of both *IMAGE* and *Geotail*. Broader

longitudinal beaming is possible in principle, but temporally extended *TMRB* emission distinct from other *TMR* components (as discussed later) does not seem to be a common occurrence, implying that *TMRB* may actually be limited in longitude.

Both *IMAGE* and *Geotail* detected several of the same solar type III bursts. One burst was seen (near 7 UT) by *IMAGE* to have a low-frequency dispersive tail that extends to the *TMRB* (Figure 2 lower panel) although no such tail was detected by *Geotail* (Figure 2 upper panel). The absence of the type III tail at *Geotail* may be due to its position at the time being deep in the night-side magnetosphere (see Figure 1) and that the low-frequency tail might have been blocked by the dayside plasmasphere. The type III tail seen at *IMAGE* location, however, means that the solar wind density at the time must have been sufficiently low to allow the tail emission to penetrate the magnetosphere. The solar wind plasma frequencies from *OMNI* data (white trace in the upper panel of Figure 2) do show a near match of the lower cutoff of the first half of the *TMRB*, but they quickly exceeded the *TMRB* lower cutoff throughout the rest of the burst. This behavior essentially rules out the possibility of a solar wind source for the *TMRB*. In addition, the observations of intensity enhancement near the burst center and distinct upper frequency cutoffs by both *IMAGE* and *Geotail* argue strongly that the *TMRB* is a distinct magnetospheric emission.

The start (0830 UT) and stop (1006 UT) of the *TMRB* were both observed practically simultaneously at *IMAGE* and *Geotail* positions. While both the *IMAGE* and *Geotail* observations show the same overall frequency extent (12-50 kHz) of the burst, they also show that the burst has a lower cutoff frequency that decreases toward the center from both the beginning and end of the burst. The frequency bandwidth is also broadest at the

center of the burst where *Geotail* observations seem to extend to slightly lower frequencies. Both sets of observations clearly show no other connecting myriametric radiation, so that the *TMRB* was an isolated emission.

Figure 3 shows an expanded view of the last hour of the *TMRB* in *Geotail* data (see upper panel of Figures 2). The clearly spin-modulated burst signals shown in Figure 3 imply that the *TMRB* radiation was beamed directly from its source, although no such spin-modulation was seen by *IMAGE RPI* due to the much slower satellite spin rate (0.5 RPM) and a longer time (~ 2 min) to complete a frequency scan. The tapered shape of the frequency-time profile toward the end of the burst, particularly the lower cutoff frequencies, is quite evident and consistent with the *IMAGE* observations shown in Figure 2 lower panel. The upper cutoff frequencies, on the other hand, exhibit a number of cycles of undulations, as if the source densities were going through a series of enhancements and depletions.

Solar Wind and Magnetospheric Conditions Associated With the TMRB

A number of terrestrial myriametric radiation components are dependent on geomagnetic activity. It is therefore of interest to see what solar wind and auroral conditions are associated with the *TMRB* emission.

a) Solar wind conditions

Figure 4 plots the 5-minute solar wind, interplanetary, and auroral activity data obtained from the *NASA OMNIWeb* (*http://omniweb.gsfc.nasa.gov*). The top 3 panels in Figure 4 show the interplanetary magnetic field (*IMF*) strength, *IMF* Bz (in *GSM*) and

113 solar wind speed, respectively. These parameters show no remarkable *IMF* activity
114 before and during the entire *TMRB* interval, with 3 < *IMF* |B| < 7 nT and +1 < *IMF* Bz <
115 +6 nT. The solar wind speed in fact decreased rather steadily from 490 km s^{-1} at 0600 UT
116 to 450 km s^{-1} at 0900 UT. The positive *IMF* Bz condition throughout the interval,
117 however, may be of significance because magnetic reconnection can occur over limited
118 region poleward of the cusp [*e.g., Kessel et al.*, 1996] and could potentially provide a
119 high-latitude free energy source to produce the *TMRB*.

120 b) *Auroral conditions*

121 The lower 4 panels in Figure 4 show the *AE*, *AL*, *AU*, and polar cap (*PC*) indices.
122 Due to the positive *IMF* Bz condition during this interval, there was also no remarkable
123 substorm activity. Nevertheless auroral kilometric radiation (*AKR*) was present at the
124 beginning and the second half of the *TMRB* interval. Referring to the panels in Figure 4
125 for the *AE*, *AL*, and *PC* indices, we notice that those indices exhibit peak levels around
126 0700, 0825, and 0940 UT, consistent with the times of *AKR* activations shown in Figures
127 2. On the other hand, Figure 4 shows no apparent auroral activation during the times of
128 *TMRB*. It would seem then that if an association were to exist between *TMRB* and *AKR*
129 (or auroral activity), the two emissions at different frequency ranges are not directly
130 correlated. Figure 2 suggests that *TMRB* tends to occur after *AKR* activation.
131

132 ***Comparisons of TMRB with known TMR Components***

133 The *TMRB* appeared in the same wavelength band (10-100 km) as other terrestrial
134 myriametric radiation. The most notable ones are the different forms of continuum

radiation [*e.g.*, *Green and Fung*, 2005; *Grimald et al.*, 2008] and the auroral myriametric radiation [*Hashimoto et al.*, 1998]. We now compare the observed characteristics of *TMRB* against the known terrestrial emissions to see whether the *TMRB* might be a distinct emission.

a) *Nonthermal continuum* (*NTC*)

Classical *nonthermal continuum radiation* (*NTC*) usually appears as banded emission that extends several hours in the post-midnight to afternoon local times [*Gurnett, 1975; Gough, 1982; Green and Boardsen, 1999; Menietti et al., 2005*]. In addition, trapped *NTC* at frequencies below the magnetopause plasma frequency (~ 30 kHz) typically appears as a broadband emission due to the radiation having undergone multiple reflections within the magnetosphere [*Green and Fung*, 2005]. On the other hand, the *TMRB* beam pattern is compact, limited both in latitude and longitude and/or time (Figures 1, 2, and 3). Spin-modulations of *TMRB* shown in Figure 4 indicate that the radiation detected by *Geotail* in the night-side magnetosphere was beamed directly from the source.

Using ray-tracing calculations, *Green and Boardsen* [1999] showed that *NTC* is primarily confined to low latitudes, and ray paths reflected off the magnetopause can *rarely* pass over the polar region at Z > 5 Re. While these results are consistent with *Geotail's* position during the *TMRB* observation, spectral differences from the *NTC* and the detection of *TMRB* by *IMAGE* at high altitude (Z > 7 Re) over the high-latitude region (see Figure 1) thus make the *TMRB* likely to be an emission distinct from the classical *NTC*.

b) *Continuum enhancement* (*CE*)

Continuum enhancements are episodic *NTC* intensity enhancements that can last up to ~ 2 hours [*Kasaba et al.*, 1998]. First identified in *GEOS 2* data taken in the geosychronous region near midnight [*Gough*, 1982], and then in *IMP 6* observations in the magnetotail [*Filbert and Kellogg*, 1989], *CE* is characterized by a sudden intensification at 15-30 kHz that is followed by an overall broadening to higher frequencies and separating into discrete frequency bands (see Figure 3 in *Gough* [1982]). The band separations also widen with time. The *TMRB* spectral appearance seems to differ from *CE* by the lacking of clear frequency bands; but instead the upper cutoff frequencies exhibit some undulations toward the end of the burst (Figure 3).

Onsets of *CE* are known to temporally correspond to increases in auroral activity (*AE*, *AU*, and *AL*), including *AKR* [*Filbert and Kellogg*, 1989; *Kasaba et al.*, 1998]. As shown in Figure 2, *AKR* and *TMRB* do not have matching start times. The times of increases in auroral indices in Figure 4 are also inconsistent with the beginning time of the *TMRB*. Despite the similarity in the compact spectral appearances in the *TMRB* and the main *CE* component, the two emissions are not likely to be the same phenomenon.

c) *Kilometric continuum* (*KC*)

TMRB appears to be confined in latitude and longitude, similar to *KC* [*Green et al.*, 2004], but that might be the only similarities between the two emissions. Observed at all local times, *KC* is generated from deep inside plasmaspheric notches that rotate with the plasmasphere. The narrow latitudinal emission cone of *KC* (±15° of the magnetic equator) [*Green et al.*, 2004; *Hashimoto et al.*, 2006] can lead to different spectral appearances that depend on the observing satellite orbital characteristics. First identified

in observations by *Geotail* in a near equatorial orbit [*Hashimoto et al.*, 1999], all the *KC* discrete frequency bands lasted several hours due to the nearly synchronous changes in the emission cone and spacecraft local times [*Green et al.*, 2002; 2004], see Figure 2.3 in *Hashimoto et al.* [2006]. On the other hand, the polar-orbiting *IMAGE* satellite often observed *KC* upon crossing the magnetic equator as discrete-banded emissions with Christmas-tree patterns (*e.g.*, see Figure 2 in *Green and Boardsen*, [2006]). With the Christmas-tree center frequencies extending up to ~ 800 kHz, the emission band durations change from several hours at low frequencies (consistent with *Geotail* observations) to less than an hour at high frequencies, yielding the Christmas-tree spectral pattern. The very similar timing, frequency extents, and spectral shapes of the *TMRB* observed by *Geotail* and *IMAGE* from very different vantage points (Figure 2) mean that the *TMRB* reported here is distinct from *KC*.

d) *Auroral myriametric radiation* (*AMR*)

The *AMR*, first discussed by *Hashimoto et al.* [1994], gets its name because it occurs coincidently with *AKR* and substorm onsets. This emission is believed to be generated in the *L-O* mode above the local plasma frequency (f_{pe}) in auroral density cavities where the local electron gyrofrequency $f_{ce} > f_{pe}$. The difference in f_{ce} and f_{pe} naturally explains the difference in *AKR* and *AMR* frequency ranges [*Hashimoto et al.*, 1998]. Although *AMR* beaming can potentially account for the nightside *TMRB* observation by *Geotail*, it could not easily explain the dayside observation at high latitude by *IMAGE*. The high temporal correlation between *AMR* and *AKR* makes *AMR* an unlikely candidate for the observed *TMRB* (Figure 2).

Summary and Conclusions

We report the simultaneous observations of a terrestrial myriametric radio burst, *TMRB,* by *Geotail* and *IMAGE* from very different vantage points (Figure 1). The similarities in timing, frequency extents (12-50 kHz), and spectral characteristics of the *TMRB* seen by the two spacecraft (Figures 2) imply that the *TMRB* was a temporal emission with a fan beam radiation pattern emitted from a discrete source. The *TMRB* upper cutoff frequencies appear to exhibit undulations as shown in Figure 3. Such variability is reminiscent of the density increases and decreases as seen across field-aligned density irregularities (*FAI*). For *L-O* mode propagation, the *TMRB* undulations may suggest the presence of *FAI* in the *TMRB* source region.

The *TMRB* emission seems to occur only after *AKR* activation as shown in Figures 2 and 4, so its emission process might be a consequence of auroral activity. On the other hand, the positive *IMF* Bz condition throughout the *TMRB* interval (Figure 4) suggests that magnetic reconnection occurring over limited longitudinal range poleward of the cusp could provide a transient, high-latitude free energy source at high altitude so that the *TMRB* can be observed by *IMAGE* and *Geotail* from their respective locations (Figure1). This is consistent with the compactness of the observed *TMRB* emission pattern.

Comparisons of *TMRB* characteristics against all other known *TMR* components reveal that the *TMRB* was likely a distinct emission, although the emission mechanism might still be the same as those responsible for generating the *NTC, CE, KC or AMR*. The *TMRB* may thus be beamed radiation resulting from linear [*Jones*, 1976; *Grimald et al.,* 2007] or nonlinear mode-conversion mechanisms [*e.g.*, *Fung and Papadopoulos*, 1987], consistent with the spin-modulations seen by *Geotail*. We plan to validate this by

performing ray-tracing modeling of the *TMRB* propagation from potential source regions.

Acknowledgments

We gratefully acknowledge the *SSCWeb* and *OMNIWeb* services provided by the *NASA Space Physics Data Facility* and the use of the *OMNI* data sets.

References

Filbert, P. C., and P. J. Kellogg (1989), Observations of low frequency radio emissions in the Earth's magnetosphere, *J. Geophys. Res.*, **94**, 8867.

Fung, S.F. and K. Papadopoulos (1987), The emission of narrow-band Jovian kilometric radiation, *J. Geophys. Res.* **92**, 8579–8593.

Gough, M.P., Nonthermal continuum emissions associated with electron injections: Remote plasmapause sounding, *Planet. Space Sci.*, **30**, 657, 1982.

Green, J. L., and S. Boardsen (1999), Confinement of nonthermal continuum radiation to low latitudes, *J. Geophys. Res.*, **104**, 10,307– 10,316.

Green, J. L. and S. Boardsen, Kilometric continuum radiation, *Radio Sci. Bull.*, URSI, **318**, pp. 34-42, 2006.

248 Green, J. L. and S. F. Fung, Advances in Inner Magnetospheric Passive and Active Wave
249 Research, in *Physics and Modeling of the Inner Magnetosphere*, Geophysical Monogr.
250 155, AGU, Washington D.C., pp. 181-202, 2005.
251
252 Green, J. L., *et al.*, Association of kilometric continuum radiation with plasmaspheric
253 structures, *J. Geophys. Res.*, *109*, A03203, doi: 10.1029/2003JA010093, 2004.
254
255 Grimald, S., *et al.*, (2008), Medium-latitude sources of plasmaspheric nonthermal
256 continuum radiations observed close to harmonics of the electron gyrofrequency, *J.*
257 *Geophys. Res.*, **113**, A11216, doi:10.1029/2008JA013290.
258
259 Gurnett, D. A., The Earth as a radio source: The nonthermal continuum, *J. Geophys Res.*,
260 **80**, 2751-2763, 1975.
261
262 Hashimoto, K., *et al.*, Auroral myriametric radiation observed by Geotail, *Geophys Res.*
263 *Lett.*, **21**, 2927-2930, 1994.
264
265 Hashimoto, K., *et al.*, Source of auroral myriametric radiation observed with Geotail, *J.*
266 *Geophys. Res.*, **103**, 23475-23483, 1998.
267
268 Hashimoto, K., *et al.*, Kilometric continuum detected by GEOTAIL, *J. Geophys. Res.*,
269 **104**, 28,645– 28,656, 1999.
270

Hashimoto, K., *et al.*, Review of Kilometric continuum, in *Geospace Electromagnetic Waves and Radiation*, ed. by J. W. LaBelle and R. A. Treumann, Lecture Notes in Physics, vol. 687, Spriner, Berlin, pp. 37-54, 2006.

Jones, D., W., Source of terrestrial non-thermal continuum radiation, *Nature*, ***260***, 686-689, 1976.

Kasaba, Y., *et al.*, Remote sensing of the plasmapause during substorms: GEOTAIL observation of nonthermal continuum enhancement, *J. Geophys. Res.*, **103**, 20389-20405, 1998.

Kessel, R. L., *et al.*, Evidence of high-latitude reconnection during northward IMF: Hawkeye observations, *Geophys. Res. Lett.*, **23**, 583-586, 1996.

Matsumoto, H., *et al.*, Plasma wave observations with *GEOTAIL* spacecraft, *J. Geomagn. Geoelectr.* **46**, 59, 1994.

Menietti, J. D., *et al.*, High resolution observations of continuum radiation, *Planetary and Space Science*, **53**, 283–290, 2005.

Reinisch, B. W., *et al.*, The Radio Plasma Imager investigation on the *IMAGE* spacecraft, *Space Science Reviews* special issue on the IMAGE mission, **91**, 319-359, 2000.

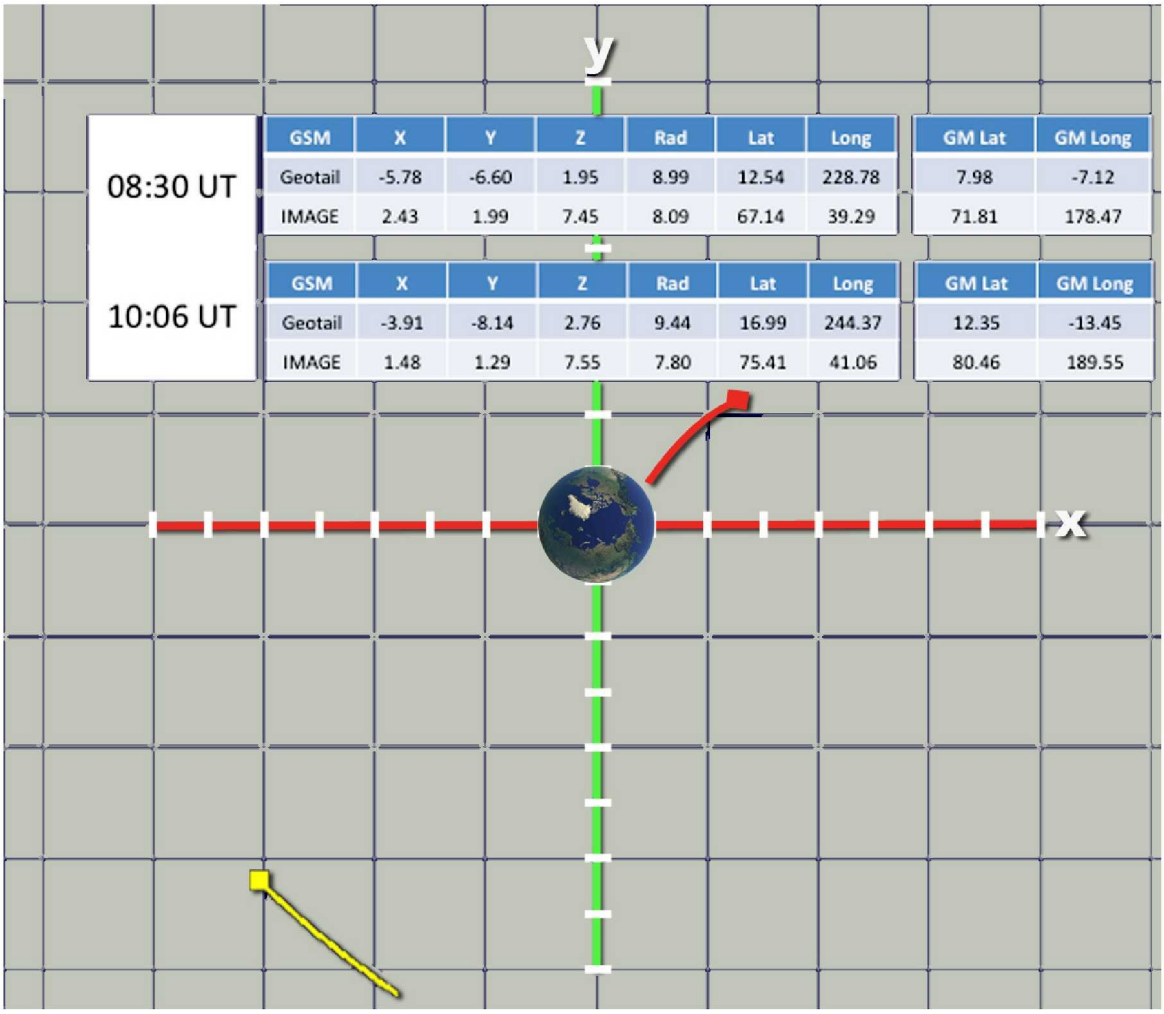

08:30 UT	GSM	X	Y	Z	Rad	Lat	Long	GM Lat	GM Long
	Geotail	-5.78	-6.60	1.95	8.99	12.54	228.78	7.98	-7.12
	IMAGE	2.43	1.99	7.45	8.09	67.14	39.29	71.81	178.47

10:06 UT	GSM	X	Y	Z	Rad	Lat	Long	GM Lat	GM Long
	Geotail	-3.91	-8.14	2.76	9.44	16.99	244.37	12.35	-13.45
	IMAGE	1.48	1.29	7.55	7.80	75.41	41.06	80.46	189.55

Figure 1. GSM and GM Positions of *IMAGE* (red) and *Geotail* (yellow) over the interval of *TMRB* observations on August 19, 2001. The two satellites were at different geomagnetic latitudes on opposite sides of the earth (*LT* ~14.6 and ~ 3.3, respectively).

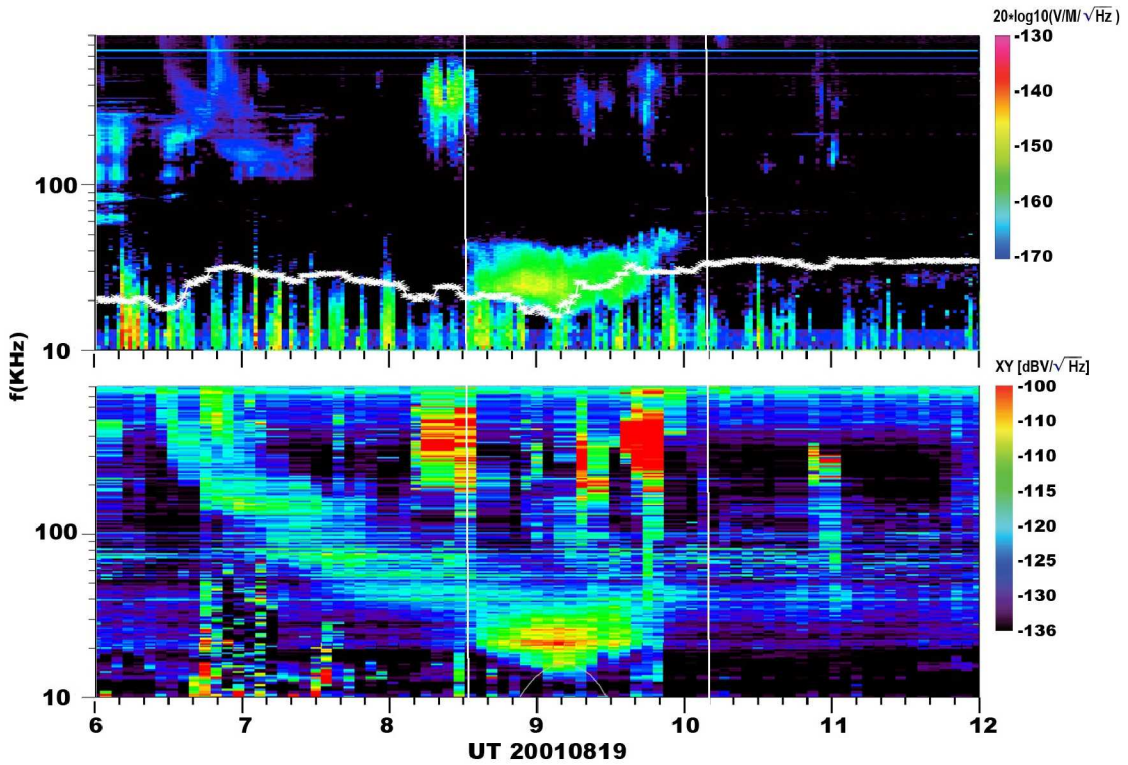

Figure 2. A 6-hour data interval showing the start and stop (demarcated by white lines) of the isolated *TMRB* being observed simultaneously by *IMAGE* on the dayside at high latitude (lower panel) and *Geotail* on the night side at low latitude (upper panel).

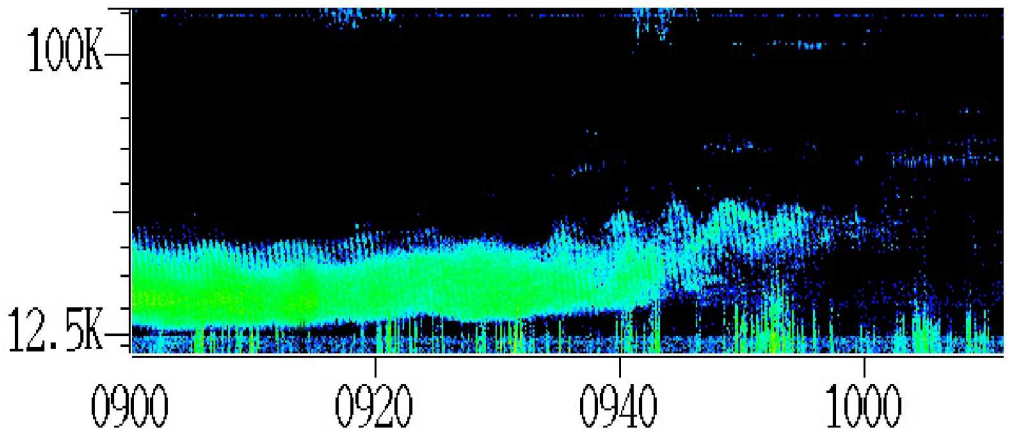

Figure 3. A 40-minute interval of *Geotail* observations covering the end of the *TMRB* at 1006 UT, showing clear spin-modulated emission and undulating upper cutoff of the burst.

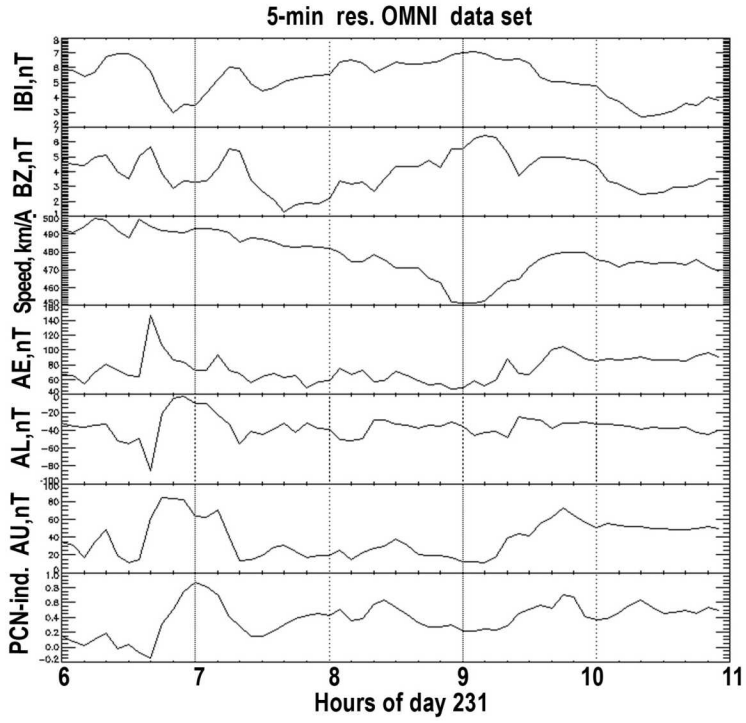

Figure 4. Solar wind and interplanetary conditions for August 19, 2001, 0600-1100 UT, covering before, during and after the *TMRB* interval.